

Analyst

Accepted Manuscript

This article can be cited before page numbers have been issued, to do this please use: A. N. Stephen and S. M. Reddy, *Analyst*, 2025, DOI: 10.1039/D5AN00663E.




This is an Accepted Manuscript, which has been through the Royal Society of Chemistry peer review process and has been accepted for publication.

Accepted Manuscripts are published online shortly after acceptance, before technical editing, formatting and proof reading. Using this free service, authors can make their results available to the community, in citable form, before we publish the edited article. We will replace this Accepted Manuscript with the edited and formatted Advance Article as soon as it is available.

You can find more information about Accepted Manuscripts in the [Information for Authors](#).

Please note that technical editing may introduce minor changes to the text and/or graphics, which may alter content. The journal's standard [Terms & Conditions](#) and the [Ethical guidelines](#) still apply. In no event shall the Royal Society of Chemistry be held responsible for any errors or omissions in this Accepted Manuscript or any consequences arising from the use of any information it contains.

1
2
3
4
5
6
7
8
9
10
11
12
13
14
15
16
17
18
19
20
21
22
23
24
25
26
27
28
29
30
31
32
33
34
35
36
37
38
39
40
41
42
43
44
45
46
47
48
49
50
51
52
53
54
55
56
57
58
59
60

Downloaded on 8/2/2025 12:56:57 PM
This article is licensed under a Creative Commons Attribution-NonCommercial 3.0 Unported Licence.


Development of a Re-usable and Disposable Sensor for the Rapid Determination of Human Chorionic Gonadotrophin (hCG) Biomarker

Andrei N Stephen and Subrayal M Reddy*,
UCLan Centre for Smart Materials, School of Pharmacy and Biomedical Sciences, University of Central Lancashire, Preston, PR1 2HE, United Kingdom
*Corresponding author: smreddy@uclan.ac.uk

Abstract

Herein we have developed a previously undescribed electrochemical nanoMIP-based sensor for the sensitive, re-usable and accurate determination of human chorionic gonadotrophin (hCG). Using a proprietary rapid and scalable method, hCG-selective polyacrylamide nanoMIP particles were produced within 2hrs at high yields of 11 mg per 1 mL reaction batch upon hCG modified magnetic nanoparticles (MNPs@CHO@hCG). The MNPs were re-usable for 5 sequential cycles of nanoMIP production. The nanoMIPs were integrated with gold screen printed electrodes by electropolymerisation within an electrochemically grown polyacrylamide layer. The ensuing hCG sensor was interrogated using cyclic voltammetry and electrochemical impedance spectroscopy. Both electrochemical modes were shown to be suitable for determining the selective binding of biomarker. The sensor was also tested using a non-target protein (SARS-CoV2 nucleocapsid protein) and was shown to be 20x more selective for target hCG compared with non-target. The linear range was shown to be 1.5 to 384 mIU with a LOD of 3 mIU and saturation occurring beyond 1000 mIU. We also electrochemically determined the equilibrium dissociation constant with EIS to be 1.4×10^{-10} M which is on a par with monoclonal antibodies produced for hCG. Sensor re-usability studies demonstrated that the same sensor once regenerated after sodium dodecyl sulphate/acetic acid treatment, could be used for 3 subsequent measurements. We present an effective method that can be used for both pregnancy testing and testicular cancer monitoring.

Keywords

solid-phase polymer synthesis; nanoMIPs; antibody; immunodiagnostics; biological extraction; magnetic nanoparticles; microwave synthesis;

Introduction

Human Chorionic Gonadotrophin (hCG) is a 36 KDa glycoprotein hormone which serves as a key biomarker for the early detection of pregnancy. Generally, hCG is first found in the maternal blood 3–4 days after initial fertilisation, with levels reaching a peak at 7–10 weeks during pregnancy¹. Most pregnancy tests measure hCG in urine within a range of 6.3 mIU/ml to 100 mIU/ml² with a positive confirmation for these tests being set at 20-24mIU. However, continuous monitoring of hCG levels is of increasing interest, as decreasing levels

Analyst Accepted Manuscript

during early pregnancy can indicate several conditions. As such a quantitative and re-usable test would benefit the end user throughout the pregnancy allowing biomarkers to be monitored more closely. The pregnancy lateral flow test for example relies on immunochromatography, where from a drop of urine on a sample pad, the pregnancy hormone human chorionic gonadotrophin, if present will bind with colloidal gold conjugated with anti-hCG antibody and diffuse on the urine liquid front through a nitrocellulose membrane to a test and control line which have been pre-modified with antibodies for hCG and antibodies against anti-hCG antibody respectively. Both lines appearing coloured indicates a positive result, whereas just the control line appearing indicates a negative result. The test is highly accurate showing positive detection rates of 99% when menstruation cycle is notably absent. Existing lateral flow tests are single-use tests which are at best qualitative only making it impossible to know if levels of hCG have changed without clinical intervention and having the blood/urine tested. The latter incurs extra cost and time commitment from a specialist. Lowered hCG levels can be a sign of an anembryonic pregnancy, where the fertilised embryo does not implant on the uterine wall³. It can also indicate a miscarriage⁴ or an ectopic pregnancy, where the fertilised embryo implants in the fallopian tube⁵. Conversely, heightened levels of hCG can arise from carrying multiple embryos⁶, molar pregnancy where the placenta fails to form⁷, or could be indicative of cancers⁸⁻¹⁰. For example, hCG can be used to detect gestational trophoblastic disease a rare group of pregnancy-related tumours that develop when trophoblast cells in the uterus grow abnormally¹¹, as well as testicular cancer in men¹². For testicular cancers, non-seminomatous germ cell tumours (NSGCT) are the type that more commonly exhibit high serum concentrations of hCG, ranging from 300 mIU/ml to 1,000 mIU/ml¹³. These heightened serum levels are observed in 40–50% of NSGCT testicular cancer patients. of those with seminomas 15–20% will show elevated levels of hCG. Among those where hCG is detected in the seminomas¹⁴, 20–40% of the 15-20% that have elevated levels will only have elevated hCG as a significant biomarker^{14, 15}.

The ability to detect hCG accurately and sensitively is therefore crucial for timely diagnosis and effective management of these conditions, making it a key biomarker to target for biosensors. Traditional methods of hCG detection come in two forms: the much more familiar and pervasive rapid lateral flow test and the enzyme-linked immunosorbent assay (ELISA). However, it is not re-usable and can give false negative readings in instances where Also, while described as rapid, with qualitative detection possible within 30 minutes, the test has the flaw of not being suitable for quantitative determination in for example cancer diagnosis and other pregnancy conditions that cause heightened levels of hCG. ¹⁶. The ELISA test is a quantitative test and while effective, is often time-consuming, labour intensive¹⁷, requiring sophisticated equipment, and is not conducive to point-of-care testing. ELISA methods also require antibodies, which must be animal-derived¹⁸; they are labour intensive and expensive to prepare¹⁹. Additionally, they need to be stored in refrigerators to maintain stability²⁰.

Epitopes are generally defined as regions of proteins to which antibodies can bind. These are typically amino acid sequences, known as peptide chains, that form part of a larger protein structure. Epitopes can be broadly categorised into two types: linear (or sequential)

1
2
3
4
5
6
7
8
9
10
11
12
13
14
15
16
17
18
19
20
21
22
23
24
25
26
27
28
29
30
31
32
33
34
35
36
37
38
39
40
41
42
43
44
45
46
47
48
49
50
51
52
53
54
55
56
57
58
59
60

epitopes, comprising a continuous series of amino acids^{21, 22}, and conformational epitopes, which consist of amino acids brought into proximity by the three-dimensional folding of the protein, despite being distant in the primary sequence^{21, 23}. Recent studies have highlighted the importance of these regions as key imprinting targets in the design of nanoMIPs.

While both whole proteins and short peptides can serve as templates in the imprinting process, whole proteins are generally considered more effective for biological applications, particularly in biosensing and drug delivery. Peptides, although easier to synthesise and handle, often fall short in several critical aspects. For example, the identification of suitable epitopes often requires extensive and systematic mapping. These are then compared against databases and ranked based on sequence uniqueness. The top-ranking epitope is subsequently synthesised and used to form the imprinted polymer²⁴. However, this approach does not guarantee that the selected epitope is the most appropriate for the target protein. Furthermore, the complexity of conformational epitopes introduces significant variability in their spatial arrangements within the protein structure. This necessitates individual optimisation of the imprinting process for each epitope, thereby increasing experimental complexity²⁵. Additionally, peptides are more prone to conformational change or degradation in solution compared to their whole protein counterparts, both in vitro and in vivo²⁶. This instability may compromise the integrity of the imprinting process. Although peptides offer practical advantages such as lower cost, increased stability, and ease of synthesis, they frequently fail to replicate the complete structural and functional context of the native protein. Other experimental methods of epitope mapping include mutational scanning, where mutations are introduced into the antigen to determine critical residues for antibody binding. This technique requires a suitable antigen to have already been identified. Protein display technologies, such as phage display, involve presenting antigen fragments on the surface of cells or viruses to identify binding regions, but again necessitate the prior purification and production of the protein. These methods often require weeks to months of laboratory work and can incur considerable costs²⁷. The use of whole proteins as templates provides a complete and unique three-dimensional conformation, which enhances the fidelity and functionality of the imprinting process. This may be attributed to cooperative effects, such as positive cooperativity, where ligand binding at one site increases the affinity at other sites. Such behaviour is typically observed in intact proteins but not in isolated epitopes^{28, 29} resulting in more effective and higher-affinity binding sites in whole protein-based nanoMIPs. For applications that demand high selectivity and specificity, whole protein imprinting remains the superior approach.

Due to concerns around antibody reliability, their animal sourcing and cost, there is a growing need to explore antibody alternatives for diagnostic applications. Molecularly imprinted polymers are gaining traction as an antibody replacement technology (ART). The technology has evolved over the past 25 years from a bulk and crude top-down approach where MIP monoliths are broken down to smaller particles^{5 30, 31} to a more refined bottom-up approach where nanoscale MIPs (nanoMIP) and thin film MIPs integrated to sensors have demonstrated high affinity for protein targets. These developments in conjunction with a rapid and low-cost method of producing high yields of such nanoMIP materials is

leading to realisation of a commercially viable ART technology with potential applications in immunodiagnostics³²⁻³⁴, biological extraction^{35, 36} and biosensors³⁷⁻³⁹. Biosensors continue to offer the promise of diagnostics that can be used by the unskilled layperson, with notable successes being the renowned blood glucose monitor and the pregnancy test kit. Our recent work⁴⁰ shows a viable alternative to current antibodies in the form of nano molecularly imprinted polymers (nanoMIPs), as high affinity synthetic antigen recognition materials. They can be produced rapidly within 20 minutes, far outcompeting antibody production times, and they exhibit nanomolar binding affinities equivalent to monoclonal antibodies while maintaining low non-specific binding, vastly reducing the likelihood of cross-reactivity, while potentially minimising false negatives. Furthermore, they demonstrate room temperature stability for a period of weeks obviating the need for cold storage. They can be integrated into electrochemical assay formats³⁷ making them a versatile and reliable alternative to current methods. Further, we have recently developed a facile method to produce high yields of nanoMIPs for biomarkers including blood proteins and the SARS-CoV-2 nucleocapsid protein⁴¹. The nanoMIPs have demonstrated their affinity and selectivity for target over non-target proteins using electrochemical sensing⁴². In this paper, we use our proprietary method to rapidly produce room temperature nanoMIPs to develop a simple and re-usable electrochemical diagnostic for hCG.

2. Experimental

2.1 Materials

N-hydroxymethylacrylamide (NHMA, 48% w/v), N,N'-methylenebisacrylamide (MBAm), ethylene glycol, iron chloride ($\text{FeCl}_3 \cdot 6\text{H}_2\text{O}$), methylhydroquinone, sodium acetate (NaOAc), phosphate buffered saline tablets (PBS, 10 mM, pH 7.4 ± 0.2), potassium ferricyanide ($\text{K}_3\text{Fe}(\text{CN})_6$), potassium chloride (KCl), sodium nitrate (NaNO_3), ammonium persulphate (APS), potassium peroxydisulfate (KPS), human chorionic gonadotropin (hCG), bovine calf serum (BCS), Sigmatrix Urine Diluent and glutaraldehyde (25% v/v) were used as received from Merck. The hCG (10,000 IU) was received as a lyophilised powder (107.4 mg), comprising 0.1 M sodium phosphate buffer and 10 mg/mL of mannitol and 1.074 mg of hCG. Recombinant nucleocapsid protein for SARS-CoV-2 was kindly donated by Dr Dalan Bailey (The Pirbright Institute, UK). Buffers were prepared in MilliQ water (resistivity $18.2 \pm 0.2 \text{ M}\Omega \cdot \text{cm}$). DropSens disposable screen-printed electrodes (Au-BT) comprising a gold working electrode (0.4 cm diameter), a platinum counter electrode and silver reference electrode were purchased from Metrohm (Runcorn, Cheshire, UK).

2.2 Instrumentation

The Anton Paar monowave 200 microwave oven for MNP synthesis was purchased from Anton Paar Ltd Hertfordshire, UK. An SLS Lab Basics centrifuge (Scientific Laboratory Supplies, Nottingham, UK) was used to separate MNP/nanoMIPs from supernatants. A Zetasizer Nano ZS DLS (Malvern Panalytical, Worcestershire, United Kingdom) was used to determine nanoMIP particle hydrodynamic diameter.

1
2
3
4
5
6
7
8
9
10
11
12
13
14
15
16
17
18
19
20
21
22
23
24
25
26
27
28
29
30
31
32
33
34
35
36
37
38
39
40
41
42
43
44
45
46
47
48
49
50
51
52
53
54
55
56
57
58
59
60

Open Access Article. Published on 15 August 2025. Downloaded on 8/20/2025 12:56:57 PM.
This article is licensed under a Creative Commons Attribution-NonCommercial 3.0 Unported Licence.



2.3 MNP Production

Bare and aldehyde functionalised magnetic particles were produced following our previously published solvothermal microwave method^{40, 43, 44}. Briefly, 0.5 g of FeCl₃·6H₂O and 1.8 g of NaOAc were dissolved in 15 mL of ethylene glycol in a 30 mL Anton Parr G30 microwave reaction vial (MRV). Glutaraldehyde (3.5 mL) was then added to the resulting solution with stirring for a further 5 min. The stirrer bar was then removed and the MRV was placed into an Anton Paar monowave 200 microwave oven and the reaction was heated up to a temperature of 200 °C with a ramp time of 18 °C/min (over 10 min). The reaction was held at 200 °C for 20 min under pressure (9 bar). The resulting composite products were allowed to cool for 10 min, washed five times with deionised water followed by two washes of ethanol, and then isolated with a neodymium magnet and then resuspended in deionised water and stored at 4 °C.

2.4 hCG Functionalization of MNPs

A suspension (1 mL) equivalent to 0.010 g of the produced aldehyde functionalised magnetic nanoparticle (MNP@CHO) was placed in an Eppendorf centrifuge tube. A neodymium magnet was placed on the side of the tube to rapidly pull the magnetic nanoparticles from the solution (10 minutes). The supernatant was removed and replaced with 1 mL of a 1 mg/mL of the lyophilised hCG powder in PBS this solution consisted of 10.74ug recombinant human chorionic gonadotrophin (hCG) equivalent to (100 IU of bioactivity) with the remaining 0.99mg of the powders weight being contributed by the mannitol. The Eppendorf was then sonicated for 2 minutes followed by vigorous shaking and vortexing to ensure the nanoparticles were fully dispersed. The reaction mixture was left undisturbed at room temperature (22 °C) for 30 minutes allowing the protein to conjugate with the MNP@CHO. After 30 minutes, the particles were once again separated from the solution and the supernatant exchanged with fresh buffer in triplicate to remove any non-conjugated protein. The resulting MNP@CHO@hCG particles thus produced were stored wet at 4 °C until further use.

2.5 NanoMIP Production using MNP@CHO@hCG

With sonication followed by vigorous shaking and vortex mixing, the magnetic nanoparticles (0.011 g) were resuspended in 906 µL of PBS (pH7.4) and transferred to a 15mL falcon tube. The tube was then placed into the thermo-mixer and set to mix at 400 rpm at room temperature. The sample was then degassed using nitrogen for 15 minutes with stirring. The nitrogen line was then removed and 37 mg of NHMA monomer (77 µL of 48% v/v solution) and MBAm (6 mg) were immediately added to the reaction mixture, followed by 40 µL of a solution containing 10% (v/v) TEMED and 5% (w/v) APS. A nitrogen headspace was then created, and the falcon tube sealed with the cap and then wrapped in parafilm. The solution was left to mix at 400 rpm for 15 minutes to allow nanoMIP particles to be produced at the surface of the MNP@CHO@hCG particles.

Analyst Accepted Manuscript

At 15 minutes, the reaction was rapidly quenched with 1 mL of 10 mM methylhydroquinone (MHQ). The reaction solution was exchanged three times with fresh PBS to remove any unreacted monomers and quencher. The solution was then resealed, and the tube placed on its side on a neodymium magnet (2 minutes). The supernatant was then removed. The MNP@CHO@hCG~nanoMIP particles were dispersed in 600 μ L of e-pure water and placed in a sonicator (using a VWR ultrasonicator (600W, 45kHz) for 5 minutes at 37 $^{\circ}$ C. The falcon tube was then once again placed on a neodymium magnet and the supernatant now containing the released nanoMIPs were placed in a 1 mL volume Eppendorf and stored at 4 $^{\circ}$ C until further use. The preparation was repeated by using MNP@CHO instead of MNP@CHO@hCG to produce non-imprinted control polymer (nanoNIP).

2.6 Integration of NanoMIP to Electrochemical Sensor

All electrochemical experiments were performed using a Metrohm Autolab PGSTAT204 potentiostat and NOVA2.1.6 software. NanoMIPs were eluted using sonication and were then entrapped within an electropolymerised layer (E-layer). E-Layers were fabricated directly onto BT-Au screen-printed electrodes (SPEs; Metrohm) using cyclic voltammetry (CV) largely following the procedure in ³⁷. Briefly, a 50 μ L solution in PBS comprising 0.1 mg of nanoMIP, 641 mM of NHMA as the functional monomer, 41.5 mM MBAm as the cross-linker, 0.29 M NaNO₃, 48.15 mM KPS was deposited onto the SPE. The potential was then cycled between -0.2 V and -1.4 V for 7 cycles at 50 mV s⁻¹ (10 min, RT, 22 \pm 2 $^{\circ}$ C) to produce the E-layer with entrapped nanoMIP. E-layers in the absence of nanoMIP were also produced as a control.

2.7 Electrochemical Studies of NanoMIP

The E-layer comprising entrapped nanoMIP islands (E-NMI) or control E-layer were exposed to varying concentrations of target protein (hCG) template solutions over a wide concentration range (1.5 mIU/mL to 10,000 mIU/mL) for a period of 5 minutes at each concentration. PBS and synthetic urine were tested as sample matrix.

Selective protein binding was tracked using either cyclic voltammetry or electrochemical impedance spectroscopy (EIS) of an external 5 mM potassium ferricyanide solution in PBS containing 0.5 M KCl as supporting electrolyte. Electrochemical impedance spectroscopy (EIS) measurements were conducted at a standard potential of 0.1 V (\pm 0.01 V) with 10 scans of frequencies, and a sinusoidal potential peak-to-peak with amplitude 0.01 V in the 0.1 - 100000 Hz frequency range. A Randles equivalent circuit was fitted for all EIS experiments using the FRA32 module (see Supplementary Fig. S1).

2.8 hCG Sensor Reusability Studies

NanoMIPs immobilised (NMI) in E-layer (See section 2.6) were produced for hCG and were tested using a solution containing 384 mIU/mL of hCG in PBS to serve as a baseline response for the sensor. This data was subsequently compared with previously produced NMI hCG

1
2
3
4
5
6
7
8
9
10
11
12
13
14
15
16
17
18
19
20
21
22
23
24
25
26
27
28
29
30
31
32
33
34
35
36
37
38
39
40
41
42
43
44
45
46
47
48
49
50
51
52
53
54
55
56
57
58
59
60

Downloaded on 8/20/2025 12:56:57 PM
This article is licensed under a Creative Commons Attribution-NonCommercial 3.0 Unported Licence.


electrodes to verify consistency across measurements and ensure the sensor’s reliability prior to conducting reusability assessments. The nanoMIP E-layer was subjected to a cleaning regimen aimed at the removal of hCG bound to the entrapped nanoMIP. This procedure involved the application of a 10% solution of SDS and acetic acid in water, based on work by Hawkins et al. (2005)⁴⁵. Post-cleaning, each regenerated sensor chip underwent a thorough rinsing process, involving three successive washes with PBS to eliminate any residual SDS and acetic acid contaminants. The effectiveness of this cleaning technique was evaluated across varying exposure times ranging from 1 to 10 minutes. Post-cleaning the electrodes were exposed to a 384 mIU/mL of hCG solution, electrochemical responses were recorded and assessed against the initial baseline responses to quantify the level of recovery achieved. This process was repeated until the regenerated electrode no longer returned to its baseline response before protein binding.

3. Results and Discussion

In our recent work⁴¹, we showed that a target protein conjugated to MNPs (MNP@CHO@protein) gave a versatile solid support for the mass production of nanoMIP. The method gave unprecedented high yields of 10 mg of high affinity nanoMIP for an equivalent mass of MNP in only a 1mL formulation. NanoMIP yield was shown to be maximised when the MNP particle size was optimal. We have extended this method here for the attachment of whole hCG onto the MNP@CHO, giving MNP@CHO@hCG. The hCG NanoMIP was then produced upon these functionalised MNP particles giving a yield of 11.26mg±0.65 for a single use of the MNP particles. Upon releasing with sonication and harvesting the nanoMIP, the remaining MNP@CHO@hCG particles could be recovered with a magnet, recycled and re-used for production of further nanoMIPs. The particles were thus re-used yielding a total of 50.3±4.1 mg of nanoMIP over 5 cycles. This method produces unprecedented levels of high affinity nanoMIP materials and is capable of further scaling for industrial (gram) level production^{40, 46}. Beyond Cycle 5, MNP particles failed to produce useful high affinity nanoMIPs due to MNP particle clumping following irreversible magnetisation of the original superparamagnetic material^{47, 48} and possible denaturation of the target protein.

Dynamic light scattering analysis of the hCG nanoMIPs (Fig. 1) indicated an average size of 205±21.4 nm making them on average 150nm larger than nanoMIPs produced for the SARS-CoV-2 nucleocapsid protein using the same protocol (See Fig S2).

Analyst Accepted Manuscript

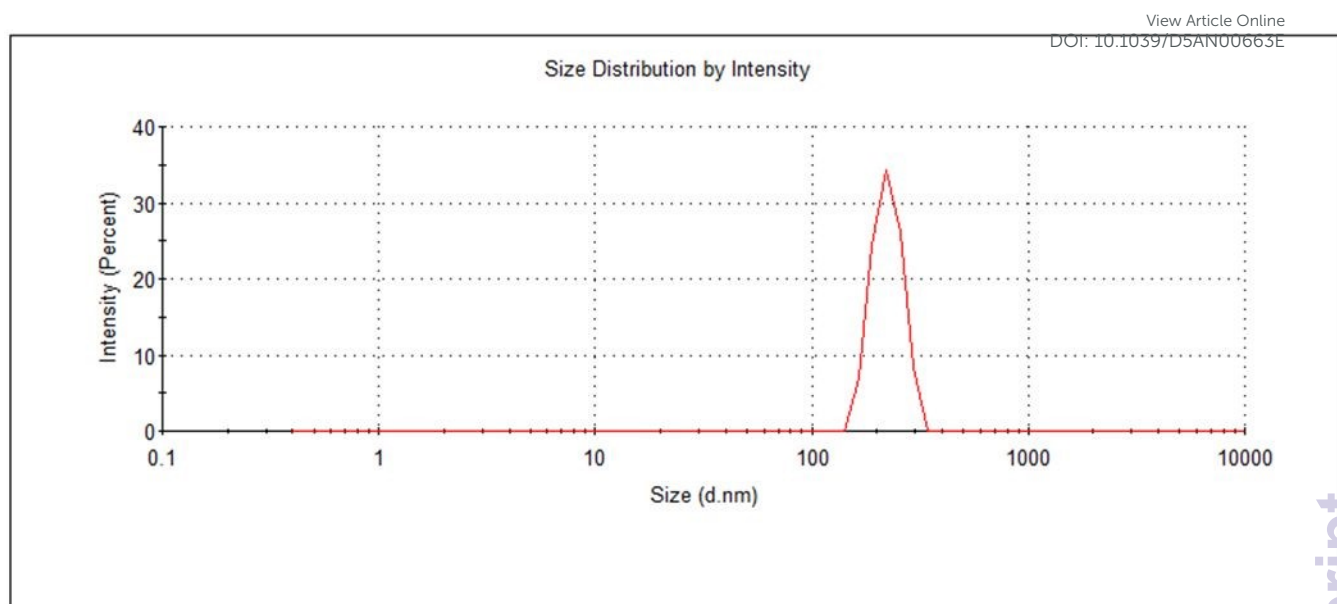


Figure 1: Dynamic light scattering (DLS) spectrum of as produced hCG nanoMIPs.

The hCG nanoMIPs were then entrapped within an electrochemically polymerised polyacrylamide phase and integrated to disposable screen-printed electrodes for subsequent electrochemical characterisation and hCG biosensor studies. NHMA monomer and bisacrylamide crosslinker were used as the precursor monomer solution for entrapping the hydrogel based nanoMIPs. In the presence of nanoMIPs, cyclic voltametric sweeps between -0.2 to -1.2 V (vs Ag/AgCl) were used to electrochemically induce radical formation from KPS initiator resulting in sulphate radicals generated locally at the electrode surface. This in turn chemically induced radical formation in the NHMA and Bis monomers at the electrode/solution interface allowing for polymer layer formation at the electrode surface while simultaneously entrapping nanoMIP at the electrode surface. Seven CV cycles were required to form an integral electropolymerised layer (Fig 2). The entrapped nanoMIP layer on SPE was stable at room temperature and while in contact with aqueous PBS when not in use to prevent the hydrogel-based biorecognition materials from drying-out and detaching from the electrode surface.

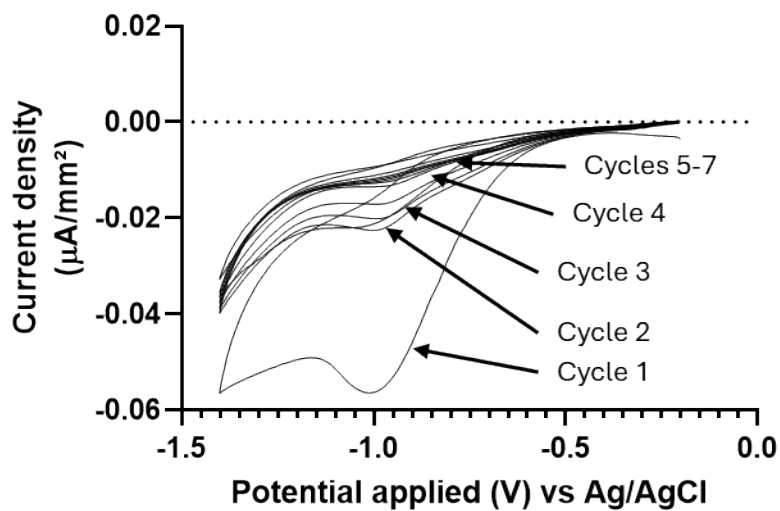


Figure 22: Cyclic Voltammograms obtained for a seven cycle E-layer deposition to physically entrap hCG nanoMIPs at the electrode surface of the Au-BT SPE.

Once the nanoMIP entrapped layer was formed, target and non-target protein rebinding was investigated electrochemically. It is generally understood that cyclic voltammetry can be used to determine micromolar concentrations of protein⁴⁹. To achieve nanomolar to sub-nanomolar protein sensitivity, application of electrochemical impedance spectroscopy (EIS) has been growing in popularity^{42, 50-55}. In either case, a model redox marker such as ferro/ferri-cyanide is required to indirectly quantify the protein levels. Both electrochemical methods were used to investigate the widest dynamic range for hCG determination (0.001-1000 IU, equivalent to 4 fM – 1nM).

Fig 3 and Fig 4 compare the responses obtained using CV (Fig 3a) and EIS Nyquist plots (Fig 4a). The corresponding calibration plots are shown in Fig 3b and Fig 4b respectively. In either case there was a concentration dependent change in electrochemical parameter measured which is directly related to detection of the ferrocyanide redox marker after each protein concentration loading. It should be noted that after each protein addition, the layer was rinsed with buffer before testing the change in molecular permeability (by CV) or change in charge transfer resistance (by EIS) to the presence of a constant concentration (5 mM) of ferrocyanide redox marker.

From the CV data (Fig 3a), the magnitude of change in peak cathodic current between the post polymerisation baseline signal and after each loading of hCG biomarker (ΔI_{pc}) is presented in Fig 3b. The inset shows the calibration plot at the lower concentration end (1-500 mIU hCG). As the protein loading increases there is a decrease in ΔI_{pc} . Beyond 1000 mIU hCG there is a plateauing of the response, likely due to saturation of the nanoMIP binding sites.

Fig 4a gives the Nyquist plots showing the change in EIS spectrum with increasing concentration of hCG (20-500 mIU) binding to the nanoMIP layer. The charge transfer resistance (R_{CT}) can be defined as the diameter of the semi-circle formed in the real impedance (Z') represented by the x-axis. We do not observe a complete semicircle because the frequency domains of effective charge transfer and diffusion overlap⁵⁶. Ideally, a Nyquist plot for a simple electrochemical system presents a perfect semicircle, representing a single charge transfer resistance and double-layer capacitance. However, the introduction of an insulating or partially insulating polymer layer, such as the NMI layer can introduce additional resistive and capacitive elements due to electronic conductivity. This often results in depressed semicircles or distorted arcs in the high-to-mid frequency region of the plot as seen in Figure 4a. The polymer layer can hinder electron transfer at the electrode surface, leading to an increased interfacial resistance and the appearance of constant phase element (CPE)-like behaviour rather than ideal capacitive phase element response⁵⁶⁻⁵⁸.

Derived from the EIS data (Fig 4a), the magnitude of change in the R_{CT} between the post polymerisation baseline signal and after each loading of hCG biomarker (ΔR_{CT}) is presented in Fig 4b. The inset shows the calibration plot at the lower concentration end (1-500 mIU hCG). That the R_{CT} increases with increasing hCG concentration suggests an increased binding level of biomarker to the nanoMIP entrapped E-layer and a subsequent reduced resistance to charge transfer of ferrocyanide redox marker at the electrode surface. Fig. 4b demonstrates the dynamic linear range (3-1000 mIU) and limit of detection (1.5 mIU) achieved when using EIS. This range was chosen as it represents the normal range seen between 3-4 weeks of pregnancy and is analogous with current pregnancy tests. There is no significant response in the range of 1.5-3mIU with the first notable change in R_{CT} being at 6 mIU. Background blood hCG level is 5mIU in non-pregnant women which means our biosensor is less likely to return a false positive result at the lowest concentration of hCG in real samples. At higher biomarker concentrations (1000-100,000mIU) there was a plateauing in R_{CT} response due to saturation of binding sites on the nanoMIP layer suggesting that EIS analysis is suitable for pregnancy testing but also a suitable sensing system for quantifying the very high levels of hCG present during the cancer disease states.

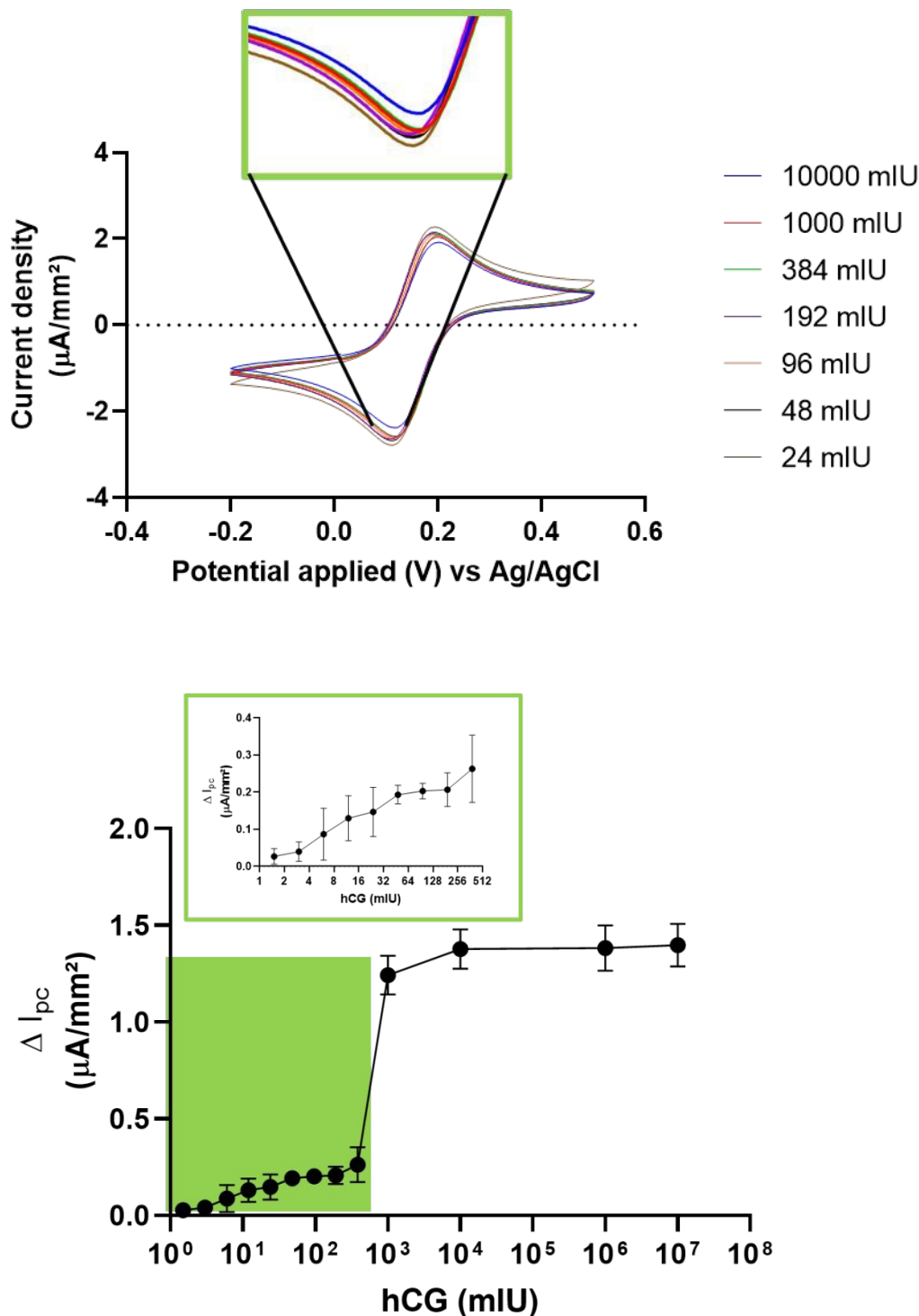


Figure 3a: Current change (measured using cyclic voltammetry) of E-Layer entrapped hCG nanoMIPs following rebinding of hCG at 24-10000 mlU. Inset demonstrates the increase in peak cathodic current with increasing hCG levels within the lower concentration range.

Figure 3b: hCG levels in mlU plotted against peak cathodic current change (ΔI_{pc}). Inset demonstrates the concentration dependent response range (1.5-384 mlU). As the hCG concentration increases, ΔI_{pc} increases proportionately until saturation of nanoMIP binding sites is reached.

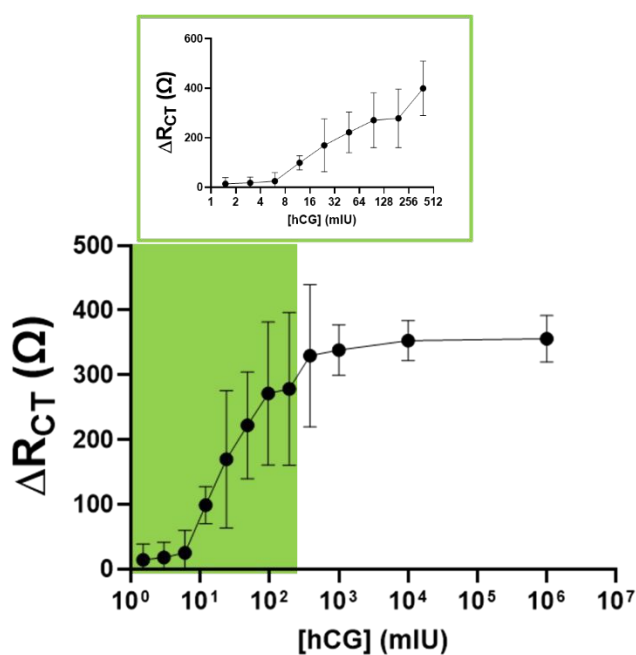
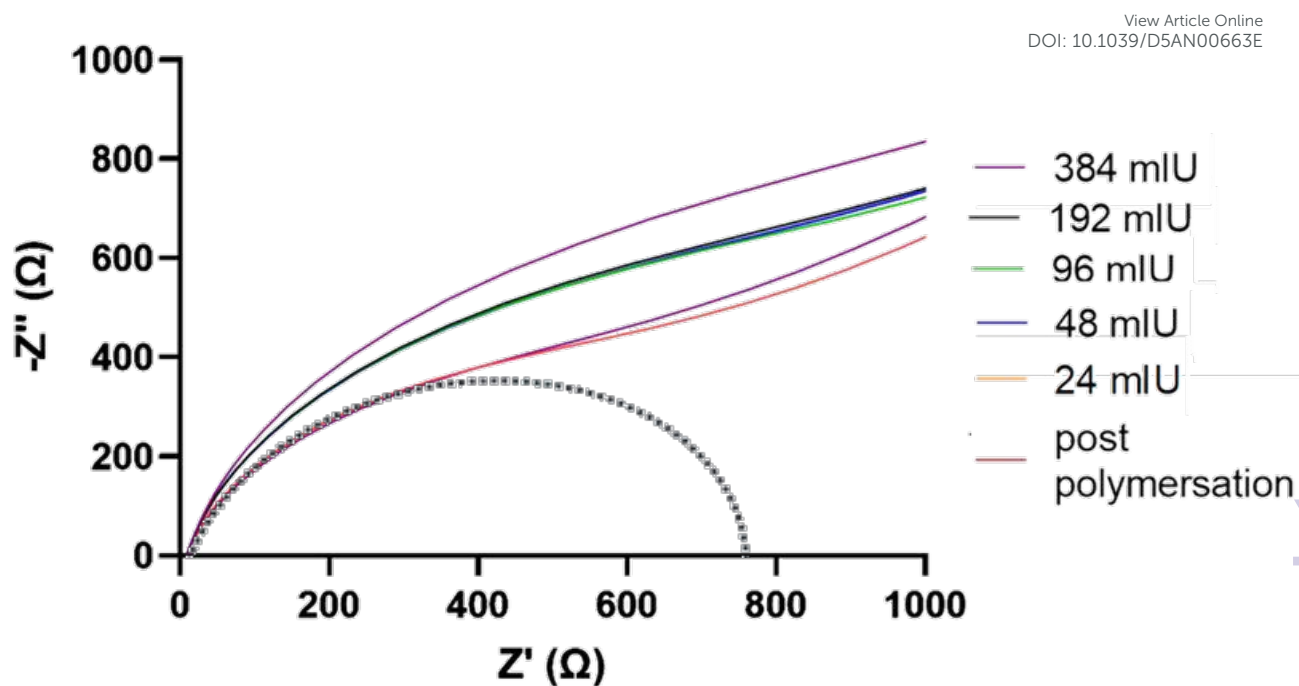


Figure 4a3: Nyquist plots for E-layer entrapped hCG nanoMIP when exposed to a range of hCG concentrations. The derived R_{CT} is equivalent to the diameter of the pseudo semicircle extrapolated from the Nyquist plot at each concentration (example semicircle given in the form of the dotted line).

Figure 4b: Calibration curve of hCG levels vs ΔR_{CT} . Demonstration of linear range for E-Layer entrapped hCG nanoMIPs exposed to hCG in PBS between 1.5-384 mlU. As the hCG concentration increases, ΔR_{CT} increases proportionately until saturation of nanoMIP

1
2
3
4
5
6
7
8
9
10
11
12
13
14
15
16
17
18
19
20
21
22
23
24
25
26
27
28
29
30
31
32
33
34
35
36
37
38
39
40
41
42
43
44
45
46
47
48
49
50
51
52
53
54
55
56
57
58
59
60

Open Access Article. Published on 05 August 2025. Downloaded on 8/24/2025 12:56:57 PM.
This article is licensed under a Creative Commons Attribution-NonCommercial 3.0 Unported Licence.



binding sites is reached. Error bars represent standard deviations for averaged signals from 3 separate electrodes.

View Article Online
DOI: 10.1039/D5AN00663E

EIS is particularly advantageous at low analyte concentrations due to its high sensitivity to interfacial changes at the electrode surface. The charge transfer resistance (R_{CT}), which reflects how effectively an electrode can oxidize or reduce a species (eg. ferricyanide/ferrocyanide couple)⁵⁶, increases when there is an insulating layer deposited on the surface, the case where the nanoMIPs are deposited on the electrode surface within an electrochemically grown layer (E-layer). The R_{CT} then increases further when the hCG binds to the entrapped nanoMIPs. This biomarker binding contributes to the insulating layer effect and further impedes electron transfer between the electrode and the electrolyte. EIS is highly effective at detecting these subtle surface changes, making it ideal for sensing at low concentrations where even minimal analyte presence leads to measurable impedance shifts. However, as more of the hCG binds to the nanoMIP layer and the surface becomes saturated, the layer insulating effect reaches a limit and plateaus. Additional binding no longer significantly alters surface properties, and EIS becomes less responsive. CV measures the current generated by the redox reaction of the permeating ferricyanide/ferrocyanide couple. As more target protein binds, less of the redox couple can access the electrode surface, resulting in a reduction of the peak anodic (I_{pa}) and peak cathodic (I_{pc}) peak currents. Since these redox species are small molecules, they may still diffuse through the insulating E-layer component of E-layer entrapped nanoMIP layer system to a limited extent, which likely explains the signal plateau at the highest analyte concentrations where all available nanoMIP binding sites are filled, but some electrolyte remains trapped between the nanoMIP/electrode interface or diffuses through the hydrogel layer. In summary, EIS is better suited for low-concentration detection due to its sensitivity to surface changes, while EIS and CV can be effective at higher concentrations.

Based on the molecular weight of the whole intact hCG (36 kDa), and that 5000 IU has been previously determined to be equivalent to 500 μg of hCG⁵⁹. We adapted the data from Figures 3b and 4b and converted the levels of hCG from mIU to mol L^{-1} (see Supplementary Figs S3 and S4 respectively), and then the Hill-Langmuir equation^{37, 60-62} was applied to determine an effective equilibrium dissociation constant (K_D) for the nanoMIP. Based on the concentration of protein required to saturate the hCG nanoMIP represented by the plateau in Fig. 3b and 4b (referred to as B_{max}), we can use the E-layer sensor results to determine a binding affinity (K_D) using the Hill-Langmuir adsorption isotherm model (ie $K_D = \text{concentration of protein at } B_{\text{max}/2}$) for the nanoMIPs produced. We assumed the Hill coefficient is equal to 1, which is indicative of ligand (MIP) binding with no cooperativity to one site. K_D was determined to be 1.73×10^{-9} M using CV data (Fig. 3b) and 1.14×10^{-10} M using R_{CT} data (Fig. 4b), both demonstrating K_D values akin to monoclonal antibodies for hCG⁶³. We observed a factor of 10 difference here likely due to the difference in determination of B_{max} , the point at which saturation is reached between the two electrochemical modes of interrogation. At high concentrations (between 10^3 to 10^6 mIU), near saturation point, for CV, $\Delta I_{pc} = 0.01 \mu\text{A}/\text{mm}^2/\text{decade}$ whereas for EIS, saturation had been reached giving $\Delta R_{CT} = 0 \Omega/\text{decade}$.

Analyst Accepted Manuscript

Figure 5 compares the EIS-derived calibration plots for hCG (1-500 mIU) obtained in PBS and synthetic urine (S-urine). The response is reduced in S-urine suggesting potential interference from the biomatrix. However, at concentrations of 32 mIU – 384 mIU the sensor nonetheless demonstrates that a quantifiable response can be obtained without the need for any dilution of the spiked urine sample. Compared with PBS responses, the overall obtained resistances in S-urine with a positive measurement are reduced by 82% at the lowest concentration to 46% reduced at the highest concentration suggesting the matrix has a significant effect on the binding of hCG and thus the ability to be selectively up taken by the nanoMIP binding sites. The synthetic urine is known to have a pH range of 6.8-7.2 which is much more of an acidic environment than the narrow neutral range of 7.4 in the PBS. hCG is known to become denatured at low pH and in the presence of high urea concentrations (a chaotropic agent [26] such as those seen in urine samples. These factors that are replicated in the synthetic urine may mean that the reduced response is due to a level of denaturation of the hCG which would cause its shape and structure to change preventing effective binding within the nanoMIP binding sites and consequently causing a reduced response. However, the fact that there is still a response means there is enough intact and recognition of hCG overall for there to be a positive response from the sensor allowing this sensor to be used within real urine samples without the need for dilution.

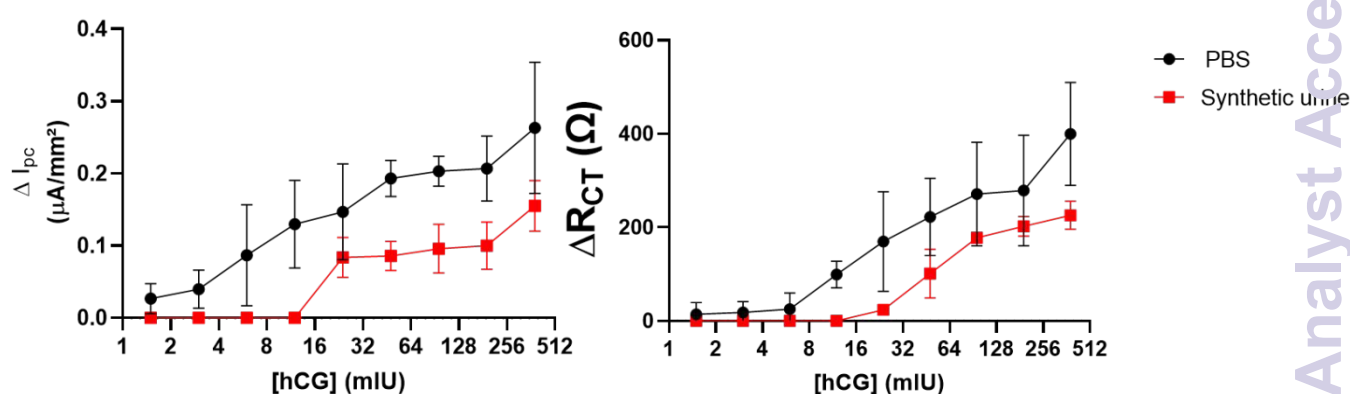


Figure 5: Peak cathodic current change (Fig 5a) and charge transfer resistance change (Fig 5b) of E-Layer entrapped hCG NanoMIPs in the pregnancy and testicular cancer relevant concentration range of hCG in PBS (black) and in a synthetic urine matrix (red) to simulate hCG in urine. Error bars represent standard deviations for averaged signals from 3 separate electrodes

The hCG nanoMIP E-layer was also tested with a model serum sample (bovine calf serum) spiked at 1000 mIU of hCG (see Supplementary Fig. S5). A near 100% recovery was observed based on relative ΔR_{CT} responses when serum was compared with PBS and S-urine matrices demonstrating that the serum did not present any matrix effects in terms of for example,

1
2
3
4
5
6
7
8
9
10
11
12
13
14
15
16
17
18
19
20
21
22
23
24
25
26
27
28
29
30
31
32
33
34
35
36
37
38
39
40
41
42
43
44
45
46
47
48
49
50
51
52
53
54
55
56
57
58
59
60

non-specific protein binding to the nanoMIP E-layer surface and/or destabilising the spiked hCG biomarker.

Based on the molecular weight of the whole intact hCG (36 kDa), and that 5000 IU has been previously determined to be equivalent to 500 μg of hCG⁵⁹ we determined that 1000 mIU was equivalent to 2.89 nM hCG. The hCG nanoMIP entrapped E-layer was challenged with SARS-CoV-2 nucleocapsid protein (N-protein) as a non-target protein of a similar size and at the same concentration as target hCG. Fig 6 shows the ΔR_{CT} differences between target and non-target binding at $1\mu\text{M}$ of biomarker (equivalent to 3460 mIU) which is at levels where all binding sites will be occupied. By taking a ratio of the two signals we determined a high selectivity factor of the nanoMIP for target hCG to be 22:1 in PBS and 20:1 in synthetic urine. While a low K_D of between 10^{-9} to 10^{-10} M gives an indication of tendency of the nanoMIP to tightly bind with the target with affinities akin to a monoclonal antibody, the selectivity factor is an effective measure of how more effective the MIP is at picking out its target protein (complement) compared with a non-target (non-complementary) protein.

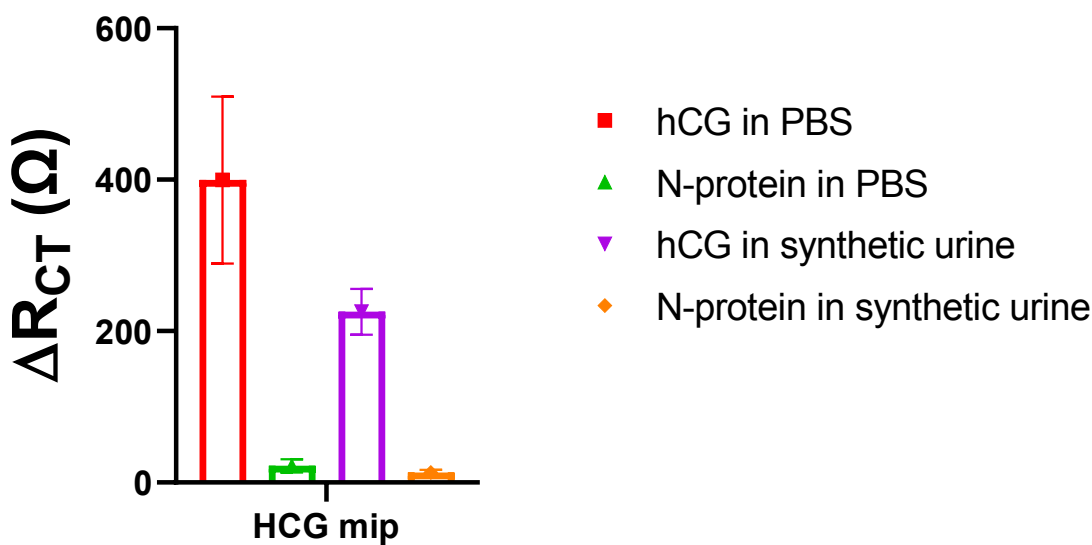


Figure 64: ΔR_{CT} response of the E-layer entrapped hCG nanoMIP to a non-target protein (SARS-CoV-2 nucleocapsid protein) compared with the target hCG biomarker. Ferri/ferrocyanide was used as redox marker to measure changes in R_{CT} .

Sensor re-usability was tested in PBS. This was achieved by removing the sensor after target binding (at 1000 mIU) and then dipping the sensor in a 10% solution of SDS and acetic acid. Sonication to removing bound protein was considered but due to the fragile nature of the physically entrapped nanoMIP, there was concern that sonication would detachment of the nanoMIP from the electrode. SDS/AcOH treatment effectively denatured and removed the selectively bound biomarker allowing the nanoMIP chip to be regenerated⁴⁵. The chip was subsequently washed with de-ionised water and PBS before re-testing with target. Fig 7

shows the R_{CT} change signals for repeat target bind and sensor regeneration. One chip could be re-used for three sequential measurements with no deterioration in signal. However, at the 3 regenerations (protein removal) of the E-MIP chip, it appeared that not all the protein could be removed. There was also a corresponding cumulative signal at the subsequent target bind stage which was no longer proportional to the concentration of target added.

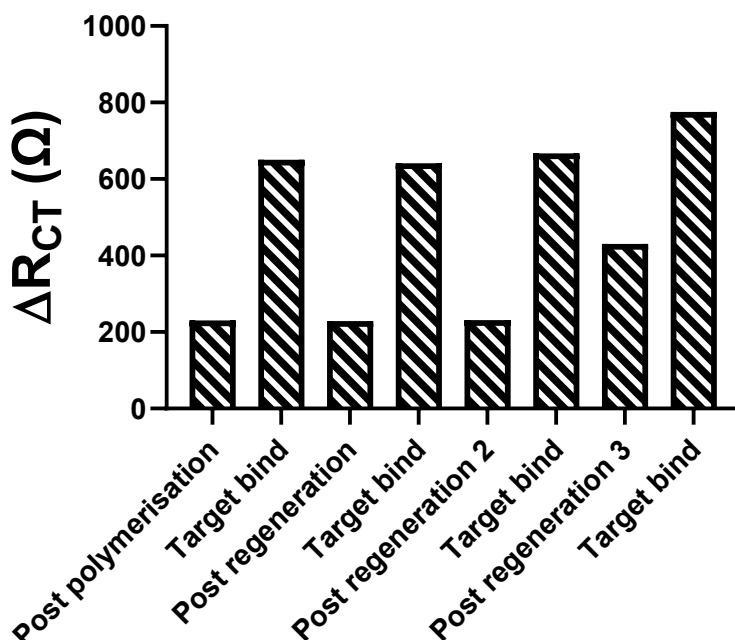


Figure 75: ΔR_{CT} response of the E-layer entrapped nanoMIP sensor showing that a single sensor can be re-used at least three times before degradation begins to occur. The ferri/ferro-cyanide couple (5mM) was used as redox marker to measure R_{CT} .

It should be noted that Figs 4b and Fig 5 represent averaged responses from three separate electrode chips. The higher standard deviations observed in Figures 4a and 5 are due to inter-electrode variability inherent in the use of screen-printed electrodes (SPEs). Unlike measurements conducted using the same electrode across multiple trials (see Fig. 7) which show minimal variability, individual SPEs can exhibit batch-to-batch and unit-to-unit inconsistencies in surface morphology, and ink distribution, which can contribute to variability in electrochemical properties and sensing performance^{64, 65}.

The ability of the MIP-based electrochemical sensor chip to be reused 2–3 times with high accuracy and specificity represents a promising advancement. Compared to industry standards like Clearblue®, which are strictly single-use due to the irreversible nature of their chemical reactions, even limited reusability offers clear sustainability and cost advantages. Commercial reusable digital systems, such as the Zioxx Digital Pregnancy test, address reusability by incorporating a reusable electronic reader alongside disposable test sticks. However, the core sensing element in these systems remains single use. Therefore, they cannot be considered truly reusable in a chemical sense, as the sensing function relies on fresh reagents and antibodies, which must be re-introduced for each test. In contrast, our MIP-functionalized electrochemical sensor offers true reusability at the chemical level, as

1
2
3
4
5
6
7
8
9
10
11
12
13
14
15
16
17
18
19
20
21
22
23
24
25
26
27
28
29
30
31
32
33
34
35
36
37
38
39
40
41
42
43
44
45
46
47
48
49
50
51
52
53
54
55
56
57
58
59
60

Open Access Article. Published on 15 August 2025. Downloaded on 8/26/2025 12:56:57 PM.
This article is licensed under a Creative Commons Attribution-NonCommercial 3.0 Unported Licence.



the molecularly imprinted polymer (MIP) can selectively bind and release hCG without requiring replacement of biological recognition elements.

View Article Online
DOI: 10.1039/D5AN00663E

MIP-based biosensors typically demonstrate limited but stable reuse often between 2-5 cycles before signal degradation occurs^{66, 67} Therefore, the consistent performance of our sensor over 2–3 uses is realistic and competitive within the current research and commercial landscape. While this does not yet match the robustness and convenience of commercial digital electronics, it represents a significant step toward more sustainable, high-performance diagnostics.

In this paper, we are demonstrating that with our simple re-usable nanoMIP-based electrochemical sensor we can reliably determine hCG in the diagnostically relevant physiological range for both pregnancy and cancer biomarker determinations. Whereas its use in pregnancy testing proves advantageous for quantitative and repeat measurements, given that the lateral flow test for quick single-shot measurement is the market leader, it is our opinion that penetration of the every-day use market using our method could face challenges. However, where repeat quantitative measurements are required in complex pregnancy situations either for personal use or in a clinical setting, our method would be recommended. Additionally, in the cases where hCG levels can be used to indicate cancer there is no reliable devices currently available on the market. Our method reliably measures elevated hCG with a cancer positive level of up to 3 IU, which could meet this need. It is also worth noting that protein selective nanoMIPs with antibody-like affinities can be manufactured at scale within 1 day, whereas the labour intensity and costs associated with monoclonal antibody manufacture are still significantly higher⁶⁸.

4. Conclusions

In this study, we have developed a novel electrochemical nanoMIP-based sensor for the sensitive, selective, and reusable detection of human chorionic gonadotrophin (hCG). The nanoMIPs were rapidly synthesized using a proprietary, scalable method, achieving high yields and enabling reusability of the magnetic nanoparticle (MNP) templates for up to five production cycles. Integration of the nanoMIPs into gold screen-printed electrodes via electropolymerisation yielded sensors capable of detecting hCG using both cyclic voltammetry and electrochemical impedance spectroscopy (EIS), with a demonstrated limit of detection of 3 mIU and a linear detection range of 1.5 to 384 mIU. The sensors exhibited a 20-fold selectivity for hCG over a non-target protein (SARS-CoV-2 nucleocapsid protein), and an equilibrium dissociation constant (K_D) of 1.4×10^{-10} M, comparable to that of monoclonal antibodies. We have demonstrated that it is usable in a mock urine sample. Furthermore, the sensors could be regenerated and reused for at least three measurement cycles. These results highlight the potential of this platform for applications in both pregnancy diagnostics and testicular cancer monitoring. Further studies are required to demonstrate its applicability in real urine and serum samples. We demonstrate for the first time that the electrochemical-based nanoMIP system has an element of reusability with the

Analyst Accepted Manuscript

sensor becoming unreliable after three sequential uses. Further sensor stability studies are required to understand how the system performs over days and weeks.

Data Availability

All data are available within the article and its Supplementary Information files and from the authors upon request.

Author Contribution

SMR: Conceptualization, formal analysis, funding acquisition, investigation, methodology, project administration, supervision, writing - original draft.

ANS: Conceptualization, data curation, formal analysis, investigation, methodology, writing - original draft.

All authors contributed to manuscript revision, read, and approved the submitted version.

Acknowledgments

The authors are grateful to the University of Central Lancashire, the Royal Society of Chemistry COVID-19 Action fund (H20-188) and RSC Research Enablement Grant (E22-5899202825), the Daiwa Anglo-Japanese Foundation (13094/13916) and The Royal Society (IES\R3\193093) for funding this work.

Competing Interests

The authors declare that the research was conducted in the absence of any commercial or financial relationships that could be construed as a potential conflict of interest.

References

1. P. A. Nepomnaschy, C. R. Weinberg, A. J. Wilcox and D. D. Baird, *Hum Reprod*, 2008, **23**, 271-277.
2. L. A. Cole, J. M. Sutton-Riley, S. A. Khanlian, M. Borkovskaya, B. B. Rayburn and W. F. Rayburn, *J Am Pharm Assoc (2003)*, 2005, **45**, 608-615.
3. Q.-W. Nie, R. Hua, Y. Zhou, H. Li and Y.-H. Yu, *Nan Fang Yi Ke Da Xue Xue Bao*, 2017, **37**, 902-906.
4. G. Homan, S. Brown, J. Moran, S. Homan and J. Kerin, *Fertility and Sterility*, 2000, **73**, 270-274.
5. K. E. Cameron, S. Senapati, M. D. Sammel, K. Chung, P. Takacs, T. Molinaro and K. T. Barnhart, *Fertil Steril*, 2016, **105**, 953-957.
6. N. Singh, A. A. Begum, N. Malhotra, A. Bahadur and P. Vanamail, *J Hum Reprod Sci*, 2013, **6**, 213-218.
7. J. L. Nodler, K. H. Kim and R. D. Alvarez, *Gynecol Oncol Case Rep*, 2011, **1**, 6-7.
8. M. W. Schoen, A. Al-Taee and B. Jallad, *Journal of Clinical Oncology*, 2017, **35**, e22503-e22503.

9. P. Komarnicki, P. Gut, M. Cieřlewicz, J. Musiatkiewicz, A. Maciejewski, M. Czupińska, G. Mastorakos and M. Ruchała, *Cancers*, 2024, **16**, 2060. View Article Online
DOI: 10.1039/D5AN00663E
10. S. Schüler-Toprak, O. Treeck and O. Ortmann, *Int J Mol Sci*, 2017, **18**.
11. J. T. Soper, *Obstet Gynecol*, 2021, **137**, 355-370.
12. J. C. Milose, C. P. Filson, A. Z. Weizer, K. S. Hafez and J. S. Montgomery, *Open Access J Urol*, 2011, **4**, 1-8.
13. U.-H. Stenman, H. Alfthan and K. Hotakainen, *Clinical Biochemistry*, 2004, **37**, 549-561.
14. K. Mann, B. Saller and R. Hoermann, *Scand J Clin Lab Invest Suppl*, 1993, **216**, 97-104.
15. B. Saller, R. Clara, G. Spöttl, K. Siddle and K. Mann, *Clin Chem*, 1990, **36**, 234-239.
16. J. Reitz, B. C. Hartman, M. E. Chase, D. Krause and A. L. Cates, *Cureus*, 2022, **14**, e30725.
17. S. Hosseini, P. Vázquez-Villegas, M. Rito-Palomares and S. O. Martinez-Chapa, in *Enzyme-linked Immunosorbent Assay (ELISA): From A to Z*, eds. S. Hosseini, P. Vázquez-Villegas, M. Rito-Palomares and S. O. Martinez-Chapa, Springer Singapore, Singapore, 2018, DOI: 10.1007/978-981-10-6766-2_5, pp. 67-115.
18. A. C. Gray, A. R. M. Bradbury, A. Knappik, A. Plückthun, C. A. K. Borrebaeck and S. Dübel, *Nature Methods*, 2020, **17**, 755-756.
19. C. Chen, G. Zoe, C. David, L. Hong and P. and Trelstad, *mAbs*, 2025, **17**, 2451789.
20. S. Sakamoto, W. Putalun, S. Vimolmangkang, W. Phoolcharoen, Y. Shoyama, H. Tanaka and S. Morimoto, *J Nat Med*, 2018, **72**, 32-42.
21. C. Chang, in *Allergic and Immunologic Diseases*, ed. C. Chang, Academic Press, 2022, DOI: <https://doi.org/10.1016/B978-0-323-95061-9.00003-5>, pp. 43-88.
22. A. Bahai, E. Asgari, M. R. K. Mofrad, A. Kloetgen and A. C. McHardy, *Bioinformatics*, 2021, **37**, 4517-4525.
23. A. Pomés, S. A. Smith, M. Chruszcz, G. A. Mueller, N. F. Brackett and M. D. Chapman, *Journal of Allergy and Clinical Immunology*, 2024, **153**, 560-571.
24. A. M. Bossi, P. S. Sharma, L. Montana, G. Zoccatelli, O. Laub and R. Levi, *Analytical Chemistry*, 2012, **84**, 4036-4041.
25. L. Pasquardini and A. M. Bossi, *Analytical and Bioanalytical Chemistry*, 2021, **413**, 6101-6115.
26. R. G. Kay and A. and Roberts, *Bioanalysis*, 2012, **4**, 857-860.
27. T. Takeuchi and T. Hishiya, *Org Biomol Chem*, 2008, **6**, 2459-2467.
28. A. Whitty, *Nature Chemical Biology*, 2008, **4**, 435-439.
29. P. S. Pidenko, K. Y. Presnyakov and N. A. Burmistrova, *Journal of Analytical Chemistry*, 2023, **78**, 953-964.
30. D. Hawkins, A. Trache, E. Ellis, D. Stevenson, A. Holzenburg, G. Meininger and S. Reddy, *Biomacromolecules*, 2006, **7**, 2560-2564.
31. J. J. BelBruno, *Chemical Reviews*, 2019, **119**, 94-119.
32. T. Serra, S. Nieddu, S. Cavallera, J. Pérez-Juste, I. Pastoriza-Santos, F. Di Nardo, V. Testa, C. Baggiani and L. Anfossi, *Sensors and Actuators B: Chemical*, 2025, **428**, 137249.
33. C. H. Cho, J. H. Kim, N. S. Padalkar, Y. V. M. Reddy, T. J. Park, J. Park and J. P. Park, *Biosensors and Bioelectronics*, 2024, **255**, 116269.
34. K. Smolinska-Kempisty, A. Guerreiro, F. Canfarotta, C. Cáceres, M. J. Whitcombe and S. Piletsky, *Scientific Reports*, 2016, **6**, 37638.
35. T. G. Halvorsen and L. Reubsaet, *PROTEOMICS*, 2022, **22**, 2100395.
36. W. Wan, Q. Han, X. Zhang, Y. Xie, J. Sun and M. Ding, *Chem Commun (Camb)*, 2015, **51**, 3541-3544.
37. A. Stephen, S. Dennison, M. Holden and S. Reddy, *The Analyst*, 2023, **148**.
38. N. Karimian, M. Vagin, M. H. A. Zavar, M. Chamsaz, A. P. F. Turner and A. Tiwari, *Biosensors and Bioelectronics*, 2013, **50**, 492-498.
39. F. T. C. Moreira, R. A. F. Dutra, J. P. C. Noronha and M. G. F. Sales, *Electrochimica Acta*, 2013, **107**, 481-487.

40. S. M. Reddy, A. N. Stephen, M. A. Holden, W. J. Stockburn and S. R. Dennison, *Biomaterials Science*, 2024, DOI: 10.1039/D4BM00990H.
41. S. M. Reddy, A. N. Stephen, M. A. Holden, W. J. Stockburn and S. R. Dennison, *Biomaterials Science*, 2024, **12**, 5845-5855.
42. A. N. Stephen, S. R. Dennison, M. A. Holden and S. M. Reddy, *Analyst*, 2023, **148**, 5476-5485.
43. A. N. Stephen, T. Mercer, W. Stockburn, S. R. Dennison, J. E. Readman and S. M. Reddy, *Materials Advances*, 2025, DOI: 10.1039/D4MA01115E.
44. M. Sullivan, W. Stockburn, P. Hawes, T. Mercer and S. Reddy, *Nanotechnology*, 2020, **32**, 095502.
45. D. M. Hawkins, D. Stevenson and S. M. Reddy, *Analytica Chimica Acta*, 2005, **542**, 61-65.
46. A. N. Stephen, T. Mercer, W. J. Stockburn, S. Dennison, J. Readman and S. M. Reddy, *Materials Advances*, 2025, DOI: 10.1039/D4MA01115E.
47. D. Wen, T. Ralph, J. Han, S. Bradley, M. J. Giansiracusa, V. Mitchell, C. Boskovic and N. Kirkwood, *The Journal of Physical Chemistry C*, 2023, **127**, 9164-9172.
48. S. M. Reddy, A. N. Stephen, M. A. Holden, W. J. Stockburn and S. Dennison, *Biomaterials Science*, 2024, DOI: 10.1039/D4BM00990H.
49. Y. ElSaboni, J. A. Hunt, C. Moffatt and Y. Wei, *IEEE Sensors Letters*, 2021, **5**, 1-4.
50. M. O. Shaikh, B. Srikanth, P.-Y. Zhu and C.-H. Chuang, *Sensors*, 2019, **19**, 3990.
51. Y. T. Yaman, O. A. Vural, G. Bolat and S. Abaci, *Sensors and Actuators B: Chemical*, 2020, **320**, 128343.
52. P. Yáñez-Sedeño, L. Agüí, S. Campuzano and J. M. Pingarrón, *Biosensors*, 2019, **9**, 127.
53. T. S. Ramulu, R. Venu, B. Sinha, B. Lim, S. J. Jeon, S. S. Yoon and C. G. Kim, *Biosensors and Bioelectronics*, 2013, **40**, 258-264.
54. D. Mahalakshmi, J. Nandhini, G. Meenaloshini, E. Karthikeyan, K. K. Karthik, J. Sujaritha, Vandhana and C. Ragavendran, *Nano TransMed*, 2025, **4**, 100073.
55. R. Üstünsoy, T. Ertaş, H. E. Gültekin, A. F. Ergenç, B. Dinç and M. Bektaş, *Applied Food Research*, 2025, **5**, 100734.
56. E. P. Randviir and C. E. Banks, *Analytical Methods*, 2022, **14**, 4602-4624.
57. E. B. Caldon, D. W. Smith Jr and D. O. Wipf, *Polymer International*, 2021, **70**, 927-937.
58. R. Muchakayala, S. Song, S. Gao, X. Wang and Y. Fan, *Polymer Testing*, 2017, **58**, 116-125.
59. P. G. McDonough, *Fertil Steril*, 2003, **80**, 1534-1535.
60. M. I. Stefan and N. Le Novère, *PLOS Computational Biology*, 2013, **9**, e1003106.
61. *The Journal of Physiology*, 1910, **40**, i-vii.
62. A. N. Stephen, M. A. Holden, M. V. Sullivan, N. W. Turner, S. R. Dennison and S. M. Reddy, *Biomedical Materials*, 2025, **20**, 025043.
63. P. Berger, R. Kofler and G. Wick, *Am J Reprod Immunol (1980)*, 1984, **5**, 157-160.
64. R. D. Crapnell and C. E. Banks, *ChemElectroChem*, 2024, **11**, e202400370.
65. R. García-González, M. T. Fernández-Abedul, A. Pernía and A. Costa-García, *Electrochimica Acta*, 2008, **53**, 3242-3249.
66. N. Amaly, G. Istamboulie, A. Y. El-Moghazy and T. Noguier, *Journal of Chemical Research*, 2021, **45**, 102-110.
67. I. Baek, H.-S. Han, S. Baik, V. Helms and Y. Kim, *Polymers*, 2018, **10**, 974.
68. H. Mahal, H. Branton and S. S. Farid, *Biotechnology and Bioengineering*, 2021, **118**, 3468-3485.

1
2
3
4
5
6
7
8
9
10
11
12
13
14
15
16
17
18
19
20
21
22
23
24
25
26
27
28
29
30
31
32
33
34
35
36
37
38
39
40
41
42
43
44
45
46
47
48
49
50
51
52
53
54
55
56
57
58
59
60

Development of a Re-usable and Disposable Sensor for the Rapid Determination of Human Chorionic Gonadotrophin (hCG) Biomarker

[View Article Online](#)
DOI: 10.1039/C9AN00663E

Andrei N Stephen and Subrayal M Reddy*,
UCLan Centre for Smart Materials, School of Pharmacy and Biomedical Sciences,
University of Central Lancashire, Preston, PR1 2HE, United Kingdom

*Corresponding author: smreddy@uclan.ac.uk

Data Availability

All data are available within the article and its Supplementary Information files and from the authors upon request. The data will be stored on the University OneDrive secure storage system with backup capability. UCLan OneDrive facility is protected by University's standard retention policy. OneDrive allows each user to store the data generated for their project securely on their drives providing confidentiality where required. Additionally, it provides provision to share with team members when required.

Open Access Article. Published on 15 August 2019. Downloaded on 8/22/2019 12:56:57 PM.
This article is licensed under a Creative Commons Attribution-NonCommercial 3.0 Unported Licence.



Analyst Accepted Manuscript